Bioconjugate Chemistry

Article

pubs.acs.org/bc

Multifunctional and High Affinity Polymer Ligand that Provides Bio-Orthogonal Coating of Quantum Dots

Wentao Wang,[†] Anshika Kapur,[†] Xin Ji,[†,#] Birong Zeng,[†,‡] Dinesh Mishra,[†] and Hedi Mattoussi*[,†]

[†]Department of Chemistry and Biochemistry, Florida State University, 95 Chieftan Way, Tallahassee, Florida 32306, United States

[‡]Department of Material Science and Engineering, Fujian Provincial Key Laboratory of Fire Retardant Materials, Xiamen University, Xiamen, Fujian 361005, PR China

Supporting Information

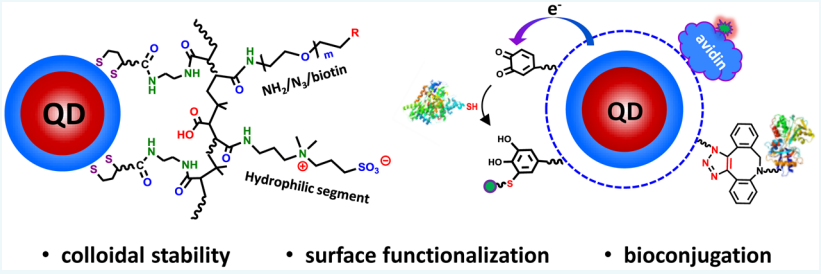

ABSTRACT: We detail the design of hydrophilic metal-coordinating ligands and their use for the effective coating of luminescent quantum dots (QDs). The ligand design exploits the specific, reagent-free nucleophilic addition reaction of amine-modified molecules toward maleic anhydride to introduce several lipoic acid metal anchors, hydrophilic zwitterion moieties, and specific reactive groups along a poly(isobutylene-*alt*-maleic anhydride) (PIMA) chain. Tunable reactive groups tested in this study include azide, biotin, carboxyl, and amine. Cap exchange with these multilipoic acid ligands via a photochemical ligation strategy yields homogeneous QD dispersions that are colloidally stable over several biologically relevant conditions and for extended periods of time. The zwitterionic coating yields compact nanoparticle size and imparts nonsticky surface properties onto the QDs, preventing protein absorption. The introduction of a controllable number of reactive groups allows conjugation of the QDs to biomolecules via bio-orthogonal coupling chemistries including (1) attachment of the neurotransmitter dopamine to QDs via amine-isothiocyanate reaction to produce a platform capable of probing interactions with cysteine in proteins, based on charge transfer interactions; (2) self-assembly of biotinylated QDs with streptavidin-dye; and (3) ligation of azide-functionalized QDs to cyclooctyne-modified transferrin via copper-free click chemistry, used for intracellular delivery. This ligand design strategy can be used to prepare an array of metal-coordinating ligands adapted for coating other inorganic nanoparticles, including magnetic and plasmonic nanomaterials.

INTRODUCTION

Luminescent quantum dots (QDs) exhibit unique photo and physical properties that are not shared by organic dyes and fluorescent proteins, and their dimensions are comparable to those of biomolecules.[1−7] These features make them very attractive for use as fluorescent platforms for imaging, sensing, and as diagnostic tools.[8−17] Regardless of what the exact final goal is, the utility of QDs in biology and medicine requires effective control over their interactions with biological systems.[18,19] Such control depends, to a large extent, on one's ability to conjugate those materials to target molecules such as proteins, peptides, nucleic acids, and drugs. Equally important is the long-term colloidal stability and the overall hydrodynamic dimensions of the nanocrystals in biological media. For example, expanded colloidal stability can improve the targeting efficiency, reduce the nanoparticle cytotoxicity, and enhance the payload binding capacity for intracellular delivery.[20,21] Similarly, compact nanocrystals provide better control over transport properties, including cellular internalization, blood vasculature circulation lifetimes, and renal clearance.[22−25] All these properties are directly affected by the nature of the capping ligands; tailoring the surface properties of nanocrystals is challenging, nonetheless.

To reduce the hydrodynamic size of QDs without sacrificing colloidal stability in aqueous media, several ligands containing zwitterion moieties (as the hydrophilic motifs) have been developed over the past few years.[25−34] Ligands based on the zwitterion motif provide nanocrystals with compact size. Additionally, to enhance the ligand affinity to the nanocrystal surface, a set of multicoordinating polymer ligands have been proposed.[25,32−41] Compared to molecular-scale ligands which can only present a few anchors, multicoordinating polymer ligands shift the adsorption/coordination equilibrium to lower concentrations, which reduces the ligand dissociation rate from

Received: June 14, 2016
Revised: July 30, 2016
Published: August 2, 2016

DOI: 10.1021/acs.bioconjchem.6b00309
Bioconjugate Chem. 2016, 27, 2024−2036

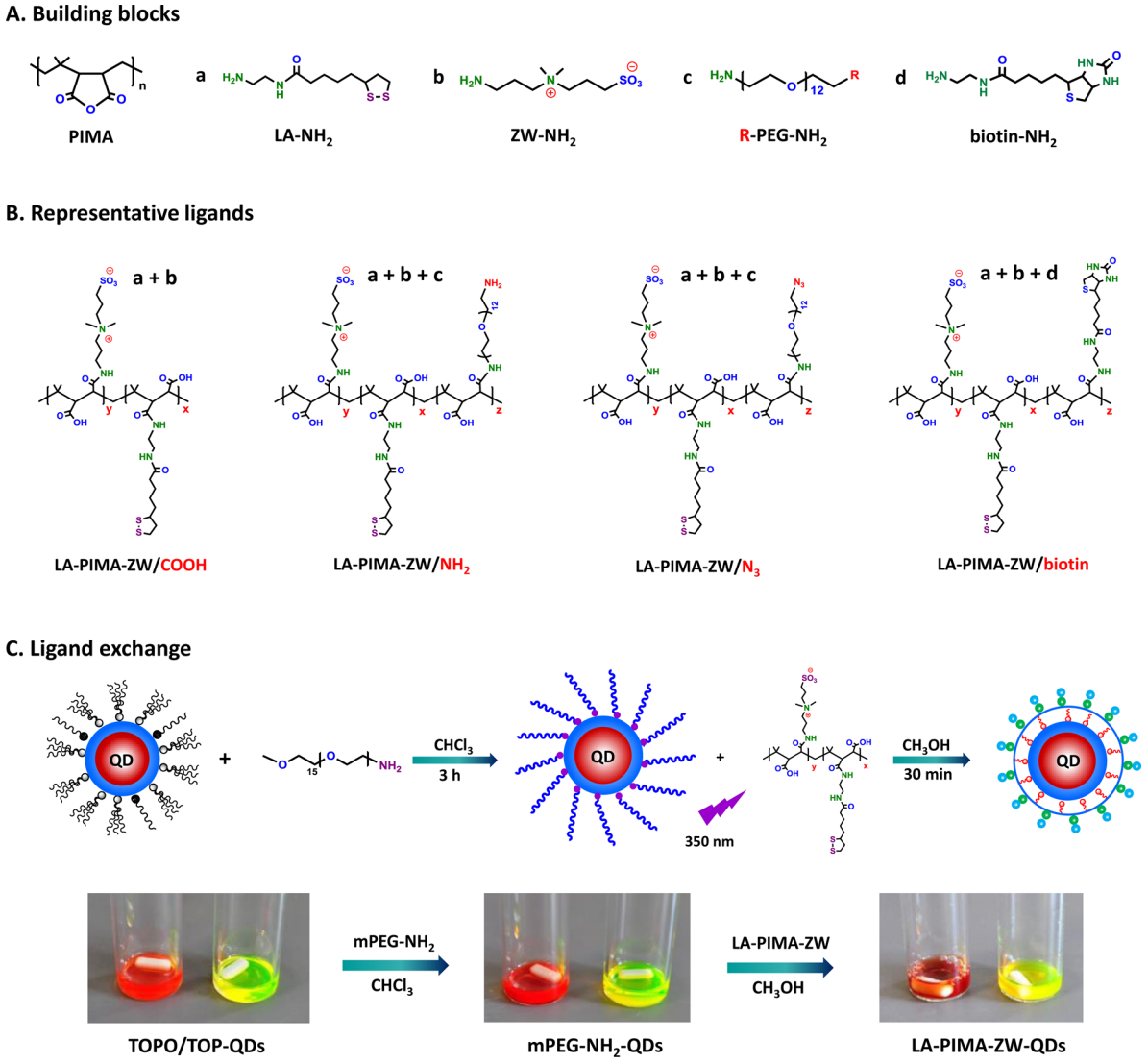

Figure 1. (A) Structures of the building blocks/precursors used in the synthesis of the polymer ligands: central PIMA scaffold; anchoring group, LA-NH_2; hydrophilic moiety, ZW-NH_2; functional group, R-PEG-NH_2 and biotin-NH_2. (B) Structures of four representative ligands are shown: LA-PIMA-ZW, LA-PIMA-ZW/NH_2, LA-PIMA-ZW/N_3, and LA-PIMA-ZW/biotin. (C) Schematic depiction of the two-step ligand exchange combined with photoligation. The white light images represent the green- and red-emitting QDs capped with TOP/TOPO in hexane (left), coated with mPEG-NH_2 in methanol (middle), and photoligated with LA-PIMA-ZW in methanol (right).

the nanoparticle surfaces, thereby greatly improving the colloidal stability of the nanocrystals.[42,43] To modulate interactions with cellular systems, designing nanocrystals that present tunable functional groups and allow decoration with target molecules, via simple bioconjugation techniques, has been vigorously pursued.[10,19,44,45]

In this study, we detail the synthesis and characterization of a set of polymer ligands that combine multiple metal-chelating groups, hydrophilic segments along with tunable functionalities (all within the same structure). We further apply them as a compact coating for QDs and test the resulting fluorescent platforms in sensor design and cell imaging. The ligand synthesis relies on the highly efficient nucleophilic addition reaction between distinct but complementary amine-presenting molecules with a short poly(isobutylene-*alt*-maleic anhydride) chain, PIMA (MW = 6000 g/mol). The resulting modular ligands present: multilipoic acid groups for strong coordination on the QD, several zwitterion moieties for water solubilization, and various reactive groups for bioconjugation (e.g., carboxyl, amine, azide, and biotin). Compared with previous ligand designs, this one-step reaction is highly efficient, reagent-free, easy to implement, and does require tedious purification of the final product(s).[28,33,36,46]

Capping the QDs with these ligands using a photochemical ligation strategy provides compact nanocrystals that exhibit long-term stability over a broad range of biological conditions, while reducing nonspecific protein absorption. In addition, this ligation strategy is gentle to sensitive groups, such as azide, which allows the assembly of QD-bioconjugates using bio-orthogonal chemistries directly on the nanocrystals. We exploited this design to apply (1) amine−isothiocyanate reaction to prepare QD-dopamine conjugates as platform for protein sensing based on charge transfer interactions; (2) biotin−streptavidin coupling which was used for ratiometric assembly of QD−dye pairs; and (3) copper-free click conjugation of transferrin to QDs, which were further tested for cell imaging. Additionally, we explored the effects of varying the nature of surface capping ligands on the self-assembly

DOI: 10.1021/acs.bioconjchem.6b00309
Bioconjugate Chem. 2016, 27, 2024−2036

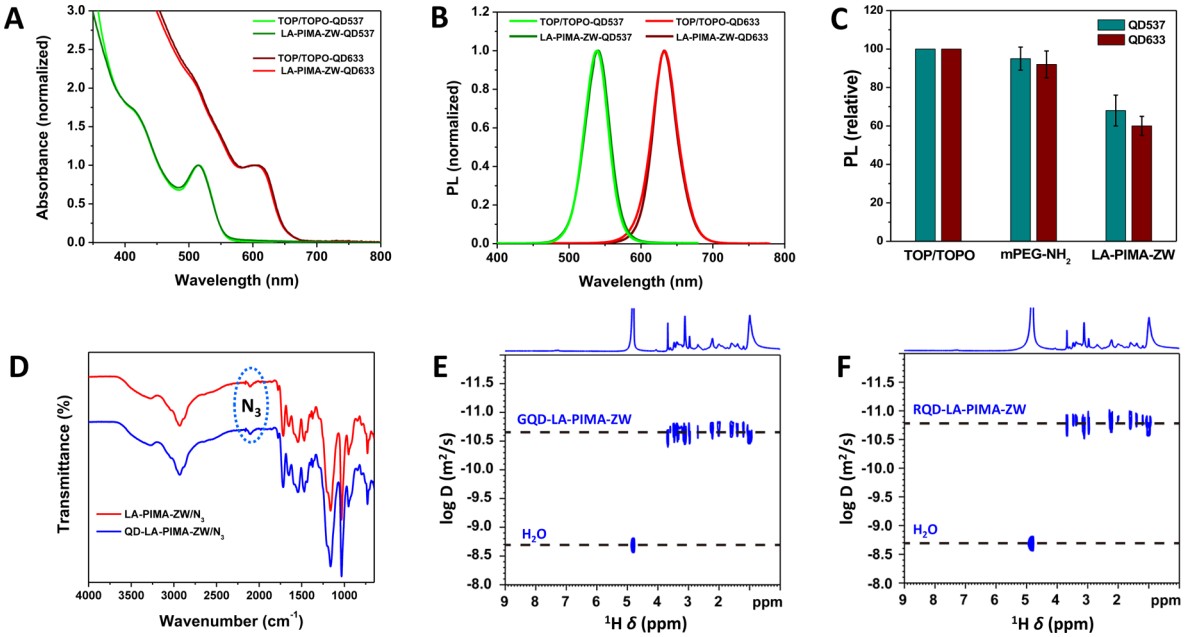

Figure 2. (A,B) Two representative normalized absorption and emission spectra collected from 537 nm-emitting and 633 nm-emitting QDs, before and after photoligation with LA-PIMA-ZW. (C) PL intensities of QDs ligated with LA-PIMA-ZW in water and mPEG-NH_2 in methanol relative to that measured for the native QDs in hexane; the same optical density is used for both samples. (D) FT-IR spectra collected from LA-PIMA-ZW/N_3 and from QDs photoligated with LA-PIMA-ZW/N_3. The band at 2108 cm^{-1} is attributed to the azide group. (E,F) Diffusion ordered NMR spectra collected from QD537 and QD633 capped with LA-PIMA-ZW in D_2O.

between polyhistidine-appended proteins and QDs. We found that conjugation is not only determined by the overall ligand lateral extension but also greatly influenced by the strength of the ligand coordination on the QDs (e.g., thiol vs imidazole).

RESULTS AND DISCUSSION

Ligand Design. The present ligand design builds on previous developments, which have shown the benefits of combining the highly efficient, one-step nucleophilic addition reaction applied to poly(isobutylene-*alt*-maleic anhydride), to prepare either amphiphilic encapsulating polymers, or metal-coordinating ligands.[34,39,47,48] We apply this chemical design to prepare high affinity multicoordinating polymer ligands that rely on the zwitterionic motif for promoting water affinity, and use them to functionalize QDs. Additionally, we exploit the simplicity of the addition reaction to engineer reactive QDs that are readily compatible with several conjugation chemistries with great utility in biology.

Figure 1A shows a summary of the amine-modified precursors used to prepare the various multifunctional polymer ligands. All ligands have been synthesized using nucleophilic addition reaction starting from the same central poly(isobutylene-*alt*-maleic anhydride) precursor/scaffold. Synthesis of the simplest ligand, LA-PIMA-ZW, was carried out by reacting the PIMA with a stoichiometric mixture of lipoic acid-amine (50%) and zwitterion-amine (50%). This is expected to introduce ~20 lipoic acid anchors and ~20 zwitterion moieties, while generating ~40 carboxyl groups along the polymer backbone. These carboxylic groups provide reactive functionalities for further conjugation and can also enhance solubility in aqueous media. When a fraction of the amino-zwitterion moieties is substituted with H_2N-R during the addition reaction, this yields a set of lipoic acid- and zwitterion-modified polymer ligands with distinct functional groups (carboxyl and R groups). Three representative ligands are shown in Figure 1B: LA-PIMA-ZW/NH_2 (carboxyl and amine), LA-PIMA-ZW/N_3 (carboxyl and azide), and LA-PIMA-ZW/biotin (carboxyl and biotin); these compounds were prepared by reacting PIMA with 10% H_2N-R together with 40% amino-zwitterion and 50% lipoic acid.

Photoligation of QDs with LA-PIMA-ZW Ligands. We have recently shown that ligation of lipoic acid-based ligands onto core−shell QDs and transfer of the materials to aqueous media can be achieved under UV irradiation.[42,49] This route relies on the in situ photochemical transformation of the dithiolane groups in the presence of the native hydrophobic QDs. This allows forgoing the need to chemically reduce LA with sodium borohydride.[42] While chemical reduction is effective, it imposes a limitation with respect to preserving the integrity of certain highly desired functional groups (e.g., azide, aldehyde, and biotin).[42,46] Photoligation in comparison is relatively mild and preserves the integrity of those functionalities. Effectiveness of the photoligation strategy stems from the photochemical sensitivity of the strained dithiolane ring to UV excitation, and it has been applied to several LA-based ligands.[28,39,42]

We, however, have found that the new polymers combing lipoic acid and zwitterionic moieties are not fully compatible with the above photoligation method, a limitation emanating from the rather stringent solubility of the zwitterion polymers. When photoligation was applied using either one-phase or two-phase configuration, the procedure yielded incomplete surface coating, resulting in poor QD stability in water. To circumvent this issue, we introduced an intermediate step in the phase transfer procedure, where the hydrophobic QDs were first ligand exchanged with methoxy-PEG-amine (mPEG-NH_2) and then the resulting QDs were photoligated with the LA-PIMA-ZW ligands. The rationale for choosing this intermediate step was based on two findings: (1) Amines are weaker metal-coordinating groups and thus can be readily replaced by

DOI: 10.1021/acs.bioconjchem.6b00309
Bioconjugate Chem. 2016, 27, 2024−2036

thiols.[38,50,51] (2) Amine-presenting ligands tend to enhance the QD fluorescence.[52] Figure 1C schematically depicts the two-step ligand exchange applied to the QDs. In the first step, the native hydrophobic shell (trioctylphosphine/trioctylphosphine oxide, TOP/TOPO) was replaced with mPEG-NH_2, driven by mass action. Capping with mPEG-NH_2 renders the QDs dispersible in methanol. This step is crucial since methanol is one of few organic solvents able to dissolve zwitterionic ligands and it is suitable for photoligation.[28,42] The white light images in Figure 1C show the dispersion of QDs in hexane (TOP/TOPO-capped), together with the dispersions of QDs coated with mPEG-NH_2 and photoligated with LA-PIMA-ZW in methanol. Images show that the intermediate phase transfer with mPEG-NH_2 combined with photoligation with the LA-PIMA-ZW yielded highly fluorescent QDs.

One interesting finding is that photoligation of the TOP/TOPO-QDs with LA-PIMA-ZW in methanol yielded homogeneous dispersion. This contrasts with our previous results when photoligation was applied to molecular zwitterionic ligands, such as LA-ZW, where a macroscopic precipitation of the QDs after UV irradiation resulted.[42] Such difference can be attributed to the solubility of the polymers in methanol, promoted by both carboxylic groups and zwitterion groups. Additionally, compared to the molecular-scale ligands (e.g., LA-ZW) smaller excess amounts of the polymer ligands are required to implement the phase transfer.[28,42,46]

Spectroscopic Characterization of the Hydrophilic QDs. Aqueous dispersions of QDs photoligated with LA-PIMA-ZW were characterized using several complementary analytical techniques: UV−vis absorption and fluorescence spectroscopy, ^{1}H NMR spectroscopy, FT-IR spectroscopy, and diffusion-ordered NMR spectroscopy (DOSY).

Optical Characterization. Figure 2A,B shows the absorption and emission spectra for two representative sets of QDs, emitting at 537 and 633 nm, before and after photoligation with LA-PIMA-ZW. The spectra of the hydrophilic QDs are essentially identical to those collected from TOP/TOPO-capped QDs dispersed in hexane, indicating that the integrity of the nanocrystals following phase transfer was maintained. Similar data were collected for QDs photoligated with LA-PIMA-ZW/R. The quantum yield of the QDs after ligand exchange was evaluated by comparing the PL intensity of hydrophilic QDs in water to those measured for the dispersions in hexane; the optical densities were maintained identical for each pair. The relative PL intensities collected from the aqueous dispersions were ∼70% for the green QDs and ∼65% for the red QDs (see Figure 2C). These values were slightly higher than those measured for QDs photoligated with LA-PEG-OMe (∼50−60%).[42] We also found that the fluorescence intensities measured for both green- and red-emitting QDs coated with mPEG-NH_2 were comparable to those recorded for their hydrophobic counterparts, indicating that the amine-terminated PEG indeed preserved high QD fluorescence.

NMR and FT-IR Characterization. The polymer-ligated QDs (in D_2O) were further characterized using pulsed-field gradient-based water suppression ^{1}H NMR spectroscopy. A typical spectrum of QD dispersions shows distinct peaks from 1.1 to 1.9 ppm, attributed to protons characteristic of the lipoic acid groups; these chemical shifts are consistent with the NMR signatures of the starting lipoic acid-amine (compare Figures S1 and S4). The pronounced resonance at 3.0 ppm corresponds to the methyl groups of the zwitterion moieties, while the broad peak at ∼0.9 ppm is ascribed to the methyl protons in the PIMA chain (compare Figures S2 and S4). In contrast, the proton signatures of the TOP/TOPO measured for the hydrophobic QDs (e.g., peaks at 0.82 and 1.23 ppm) are conspicuously absent from the spectrum of the hydrophilic QD dispersion.[39] These data clearly indicate that the native as well as the intermediate ligands have been completely displaced by the polymer ligands during the final photoligation step. In addition, we anticipate that the ligand density of polymer ligands for this type of coating to be ∼13−15 coordinated ligands per QD (green-emitting), based on prior ^{1}H NMR characterization of nanoparticles using PEG-modified PIMA ligands.[39]

We further used FT-IR spectroscopy to verify that the photoligation of the QDs could preserve the integrity of the functional groups on nanocrystals. For this, LA-PIMA-ZW/N_3 was chosen as a model due to the wide use of the azide group in click chemistry.[53] We previously attempted to prepare azide-functionalized QDs using chemically reduced DHLA-based ligands; however, our attempts were unsuccessful.[46] The main challenge has been the sensitivity of this group to chemical reduction during the transformation of LA to DHLA using $NaBH_4$. Figure 2D shows two FT-IR spectra collected from the pure LA-PIMA-ZW/N_3 ligand (red) and QDs photoligated with LA-PIMA-ZW/N_3 (blue). The spectra are identical, with a clearly defined band at 2108 cm^{-1} attributed to the azide absorption. This confirms the ability of our strategy to provide hydrophilic QDs that present intact azide groups, which can be targeted for further modification (see below). Additional proof for introducing other functional groups, such as biotin, onto the QD surface is provided in Supporting Information (Figure S5).

DOSY Characterization. Previous TEM data collected from QD materials show that the hydrophilic QDs maintain their overall size following phase transfer, with no sign of aggregation. The radii measured for CdSe-ZnS QDs emitting at 537 and 633 nm using TEM and small X-ray scattering are ∼1.5−2 nm and ∼3.5−4 nm, respectively.[54,55] TEM probes mainly the inorganic core, but can be supplemented with data on the hydrodynamic radius extracted from diffusion-ordered NMR spectroscopy (DOSY) and/or dynamic light scattering (DLS).[34] DOSY is more effective for probing small size nanocrystals than DLS, nonetheless.

DOSY is a nondestructive technique that exploits the time-dependent NMR signature of active atoms (e.g., ^{1}H, ^{13}C, or ^{31}P) in solution, and provides a measure of the translational diffusion of the overall molecule (or complex).[56] When applied to colloidal nanocrystals, DOSY allows the assignment of spectral features associated with the atoms to diffusing molecules that are either nanocrystal-bound, or free in the solution.[34] The panels in Figure 2E and F show representative two-dimensional DOSY spectra collected from QD537 and QD633 ligated with LA-PIMA-ZW in D_2O. For each spectrum we found that the various proton resonances of the polymer can be ascribed to one overall diffusion coefficient which is different from that of water molecules. More precisely, we measured a diffusion coefficient of ∼3.22 × 10^{-11} m^2/s for QD537 and ∼2.84 × 10^{-11} m^2/s for QD633, in addition to the faster diffusion coefficient (∼1.73 × 10^{-9} m^2/s) measured for water molecules. The existence of one diffusion coefficient associated with all the proton resonances indicates that QD-bound LA-PIMA-ZW ligands are tracked, with no detectable free ligands in a purified QD sample. This further confirms the effectiveness of the ligand design and phase transfer protocols used. The hydrodynamic radius (R_H) extracted from the

DOI: 10.1021/acs.bioconjchem.6b00309
Bioconjugate Chem. 2016, 27, 2024−2036

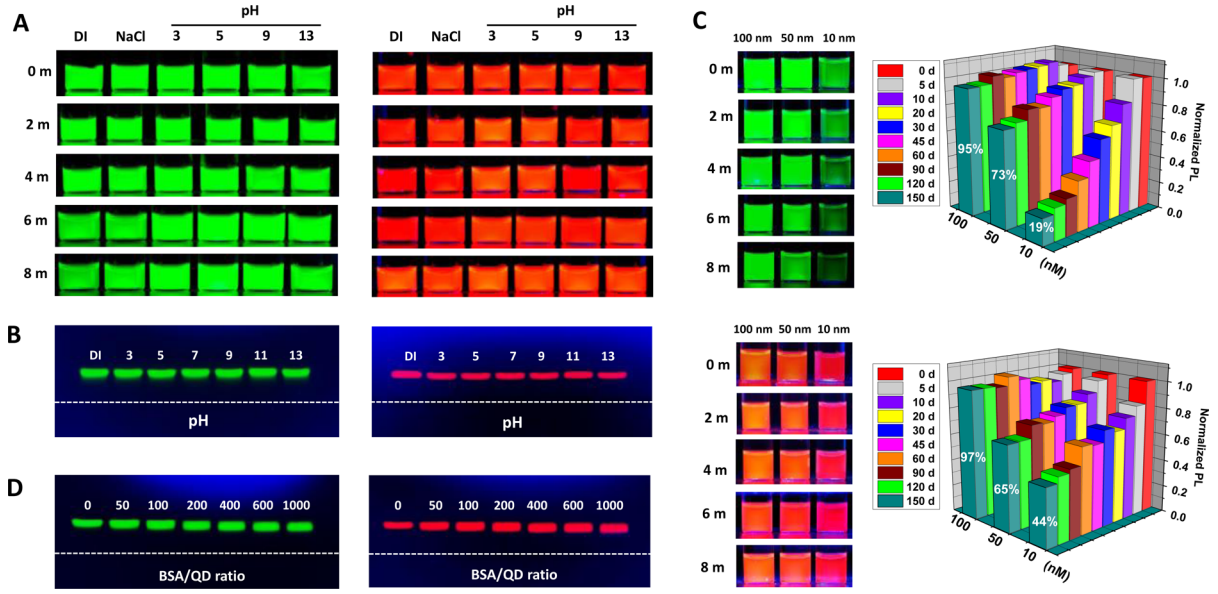

Figure 3. (A) Colloidal stability tests applied to green- and red-emitting QDs ligated with LA-PIMA-ZW: dispersed in DI water, in NaCl solution (1 M), and in phosphate buffer (20 mM) at different pH (3 to 13) over 8 month storage. (B) Images of agarose gel collected from green- and red-emitting QDs ligated with LA-PIMA-ZW dispersed in buffers at different pH from 3 to 13. The dashed line indicates the location of the wells. (C) Colloidal stability tests of the same QD dispersions at different concentrations (100, 50, and 10 nM) tracked over 8 month storage, along with time progression of the PL intensities over a 5 month period. (D) Agarose gel images of LA-PIMA-ZW capped green and red QDs incubated with different molar ratios of BSA.

diffusion coefficient data listed previously using the Stokes–Einstein equation, $D = k_B T/(6\pi\eta R_H)$, is $R_H \sim 6.6$ nm for QD537 and $R_H \sim 7.6$ nm for QD633; k_B is the Boltzmann constant, T is the absolute temperature (293 K) and η is the dynamic viscosity of the medium (~1 cP or 1.002×10^{-3} N s/m^2).[57,58] The value for the QD537 set is substantially smaller than that measured for the same QDs coated with PEGylated polymers ($R_H \sim 11$ nm), but in good agreement with the size measured for QD537 coated with His-PIMA-ZW.[34,39]

Colloidal Stability Tests. The colloidal stability of the two sets of QDs photoligated with LA-PIMA-ZW was tested under several conditions, including a broad pH range from 3 to13, high ionic strength buffer (1 M NaCl), and storage at nanomolar concentration (e.g., 10 nM). The stability of hydrophilic QDs was also evaluated in the presence of high concentration of serum albumin (up to 3.6 mg/mL), which is often used in model studies of protein adsorption onto nanoparticles. This test is valuable since nonspecific adsorption of biomolecules on the nanoparticle surfaces results in low targeting efficiency and unfavorable biodistribution.[59−63] Thus, developing "non-sticky" coating with minimal protein adsorption is paramount to the integration of these materials in biology.

Figure 3A shows the fluorescence images acquired from green-emitting and red-emitting QDs (0.3 μM) dispersed in buffers at different pH (3−13) and in 1 M NaCl solution, as-prepared and after different storage periods extending up to 8 months. All QD dispersions stayed homogeneous, with no sign of microscopic aggregation or visual loss of fluorescence for either set. The colloidal stability of LA-PIMA-ZW-QDs at different pH was further complemented by agarose gel electrophoresis, as shown in Figure 3B. The fluorescent bands measured for the QDs at pH 3−13 are narrow and all migrate toward the positive electrode with a similar mobility shift. This indicates that the dispersions are homogeneous and the QDs have negative surface charge at all pHs, resulting from the combined contribution of the carboxyl and sulfonate groups in the polymer coating.

We further tested the colloidal stability of the QD dispersions at very low concentrations. The fluorescence images in Figure 3C indicate that both sets of QDs stayed fluorescent and aggregate-free for at least 8 months at all tested concentrations (100 nM, 50 nM, and 10 nM). The intensity profiles show that the fluorescence of the 100 nM dispersion was essentially unchanged with storage time. Conversely, at 50 nM the PL intensity for both sets gradually decreased with time but remained highly fluorescent after 5 months, with relative signal of 73% for green QDs and 65% for red QDs compared to freshly prepared samples. In comparison, for the 10 nM sample, a faster reduction in PL was measured for green QDs, but the red QD dispersion exhibited better PL stability with ~45% fluorescence measured after 5 months.

Finally, we evaluate the ability of zwitterionic coating to prevent nonspecific protein adsorption and protein corona formation using a simple but sensitive assay based on gel electrophoresis. The data were further complemented with hydrodynamic radius data collected using dynamic light scattering measurements. Green- and red-emitting QDs were incubated with increasing molar ratio of bovine serum albumin (BSA) for 1 h. After incubation the samples were tested using agarose gel electrophoresis to probe potential changes in the band shape and mobility shift compared to a control sample. The images in Figure 3D show that narrow bands with similar mobility shift are measured for the nanocrystals when the BSA-to-nanocrystal molar ratio was increased from 0 to 1000 (BSA concentration ~3.6 mg/mL). The DLS measurements were limited to probing the potential interactions of BSA with green-emitting QDs to avoid interference of the red-emitting QD PL with the laser signal. Data show that when the molar ratio of BSA to QD was increased from 0 to 1000, the hydrodynamic radius of the QDs essentially remained constant ($R_H \cong 6.9$ nm was measured for all samples; see Figure S6). These results

DOI: 10.1021/acs.bioconjchem.6b00309
Bioconjugate Chem. 2016, 27, 2024−2036

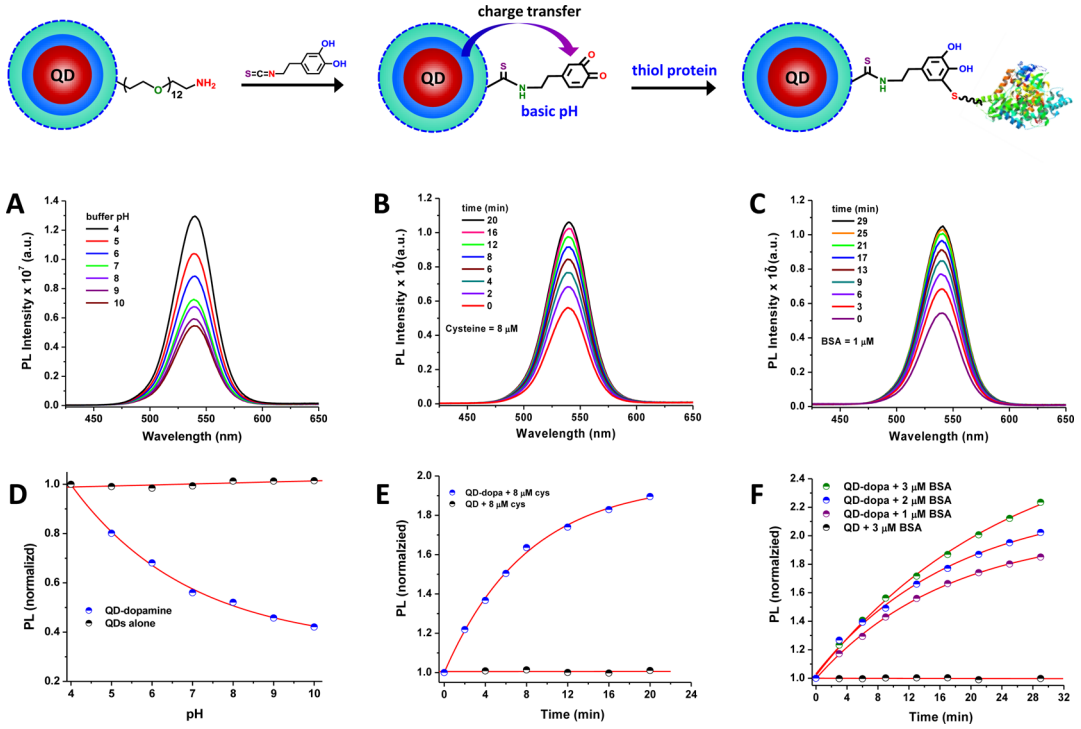

Figure 4. (Top) Schematic representation of the changes in the charge transfer interactions between the QD and proximal dopamine. (A,D) PL spectra collected from dispersions of QD−dopamine conjugates at pH ranging from 4 to 10, together with the integrated PL intensity normalized with respect to the value at pH 4. (B,E) Time progression of the PL spectra of QD−dopamine conjugates (initially dispersed at pH 10) mixed with 8 μM cysteine, together with the time-dependent integrated PL normalized with respect to the initial value at 0 min. (C,F) Time progression of the PL spectra of QD−dopamine conjugates (dispersed at pH 10) after mixing with 1 μM BSA. Plots of the progression of the integrated PL at different concentrations of BSA are also shown.

combined confirm that zwitterion coating provides hydrophilic QDs with uniform size and surface charge distribution along with "non-sticky" surface properties, thus preventing protein adsorption on the QDs.

Surface Functionalization and Bioconjugation. The utility of QDs along with other nanocrystals in biology greatly depends on one's ability to carry out conjugation to target biomolecules with control over the valence and possibly orientation.[18] This is determined by the surface functionalization and the effectiveness of the conjugation approaches used for assembling QD−bioconjugates.[8,10,19,44] Using the synthetic scheme established in this work, we have prepared several ligands presenting distinct reactive functionalities and further tested conjugation of the QDs to target molecules using a few specific coupling chemistries. These include (1) amine-isothiocyanate used to develop protein sensors; (2) biotin−streptavidin binding, applied to form energy transfer pairs; (3) copper-free click reaction, implemented using DBCO-modified transferrin and tested for intracellular delivery; and (4) polyhistidine-mediated metal-coordination to form QD-protein self-assemblies.

QD−Dopamine Conjugates for Sensing Thiol Protein. In previous studies, we have shown that conjugation of the neurotransmitter dopamine to QDs yields sensing platforms where the fluorescence emission can be modulated by charge transfer interactions between the QD and proximal dopamine.[64−66] Such platforms have been used to track pH changes and interactions with either Fe ions or the amino acid cysteine.[34,64] Here, we used QD−dopamine conjugates prepared using the new polymer coating to prove the specific coupling between the oxidized dopamine and cysteine residue in a protein.

The conjugation of QD−dopamine relied on the covalent coupling (via an isothiourea bond) of dopamine-isothiocyanate to amine groups on QDs photoligated with LA-PIMA-ZW/NH_2 as we tested and verified in our previous work.[34,64] We first examined their ability to report on pH changes and the presence of cysteine in the medium. The changes in the functional groups involved in each step were monitored and confirmed by ^{1}H NMR spectroscopy (Figure S7). Figure 4A shows the PL spectra collected from dispersions of QD−dopamine conjugates at different pH from 4 to 10. A cumulative plot of the normalized PL intensity shows a steep reduction in the QD emission when the pH was progressively shifted from acidic to basic (Figure 4D). In comparison, no change in PL was measured for the control sample made of QDs alone. This pH-induced PL loss is attributed to a change in the oxidation potential of the catechol combined with a shift in the chemical equilibrium between the catechol (electron donor) and quinone (electron acceptor) with increasing pH.[64,65] To probe interactions with cysteine, a dispersion of QD−dopamine was brought to pH 10 (quenched sample), and then an aliquot of cysteine solution was added, and the progressive increase in PL was tracked with time until saturation (see Figure 4B and E). The PL recovery can be attributed to the irreversible transformation of the quinone to 5-*S*-cysteinyl-dopamine, which reduces the charge transfer interactions in the complexes. These results are consistent with our previous findings using a different surface coating.[34,64]

We further expanded this sensing format to probe the interactions with cysteine residues within a full size protein

DOI: 10.1021/acs.bioconjchem.6b00309
Bioconjugate Chem. 2016, 27, 2024−2036

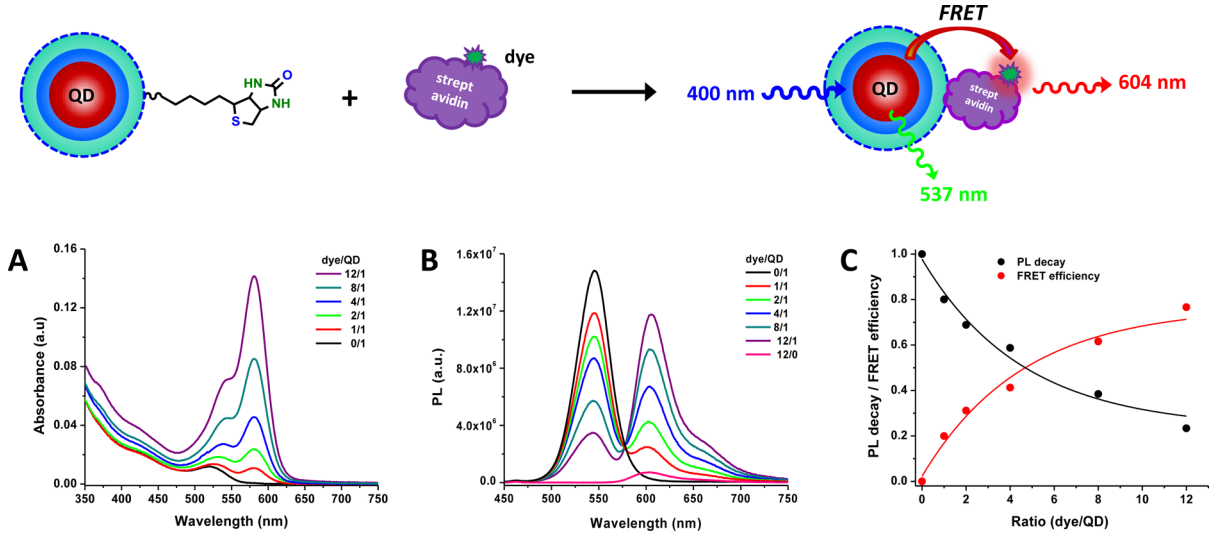

Figure 5. (Top) Schematic depiction of the self-assembly between biotinylated QDs and streptavidin-dye. (A,B) Evolution of absorption and emission spectra of QD-streptavidin-dye conjugates as a function of the dye-to-QD ratio between 0:1 and 12:1. (C) Experimental values for the relative QD PL quenching (black dot) versus valence n together with the corresponding FRET efficiency (red dot). Data were fit to a hyperbolic function in the form: $E = nR_0^6/(nR_0^6 + r^6)$. Additional details on the FRET analysis are provided in the Supporting Information.

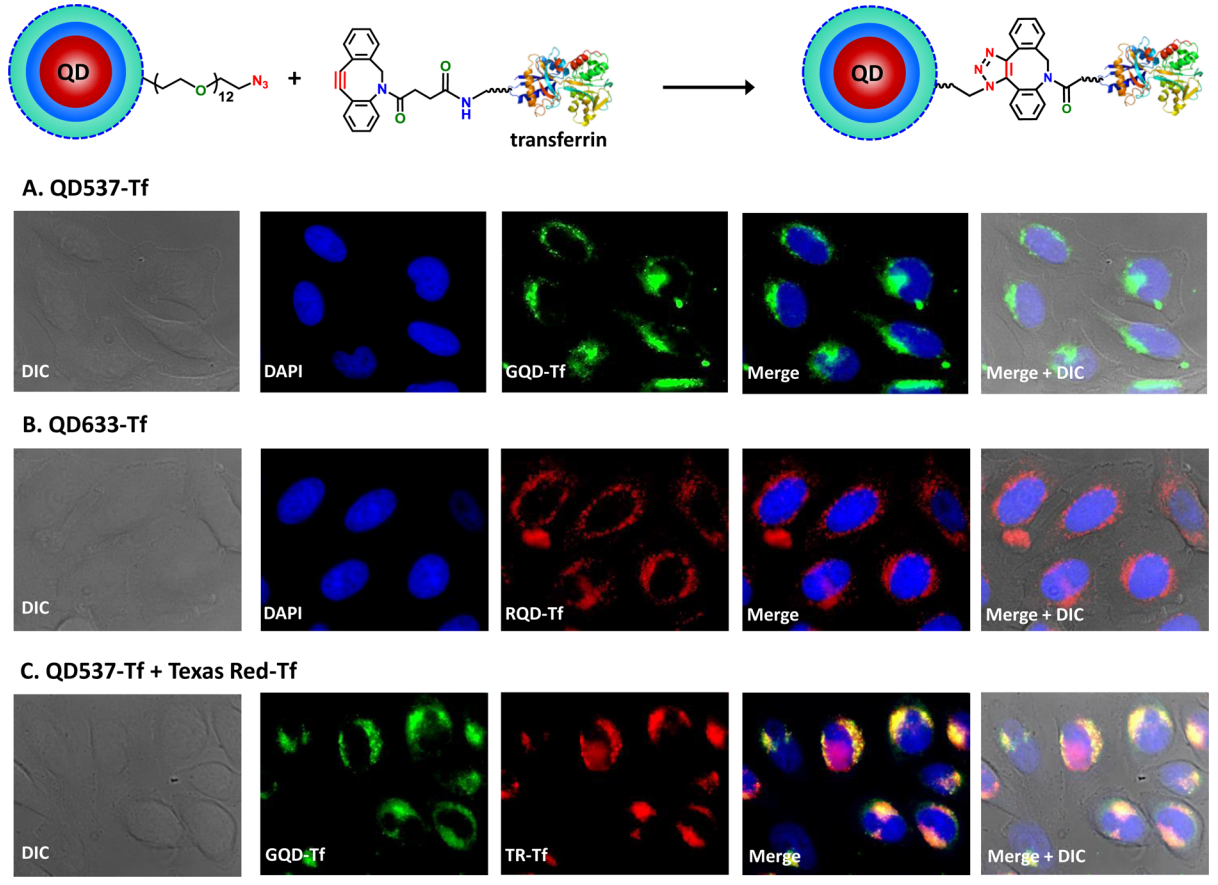

Figure 6. (Top) Schematics of the copper-free click reaction between azido-QDs and transferrin-DBCO. (A,B) Representative epi-fluorescence images collected from HeLa cells incubated with 200 nM green-emitting and red-emitting QD-transferrin conjugates for 1 h. The panels correspond to differential interference contrast (DIC), DAPI fluorescence (blue, ~460 nm), QD fluorescence (green, ~537 nm; and red, ~633 nm) and composite images combining DAPI, QDs, and DIC. (C) Fluorescence images of HeLa cells incubated with 200 nM green emitting QD−transferrin conjugates for 1 h and then with 0.5 μM Texas Red transferrin for 40 min. The panels represent the DIC, QD fluorescence (green), Texas Red−transferrin fluorescence (red, 615 nm), and composite fluorescence showing DAPI, QDs, and DIC.

(serum albumin). Serum albumin is an abundant protein in the blood and plays a major role in stabilizing extracellular fluid.[67]

Figure 4C shows the PL progression with time collected from a dispersion of QD−dopamine conjugates (at pH 10) after the

DOI: 10.1021/acs.bioconjchem.6b00309
Bioconjugate Chem. 2016, 27, 2024−2036

addition of 1 μM BSA. The PL recovery exhibited time-dependent increase until saturation after 30 min of incubation. Moreover, the PL recovery profile slightly varied with BSA concentration as shown in Figure 4F, where faster recovery was observed at higher concentration of BSA. In contrast, QDs alone (no dopamine) did not exhibit any PL changes in response to added BSA. The formation of conjugates between QD−dopamine and BSA was also verified by agarose gel electrophoresis, where a clear mobility shift of the fluorescent band was measured following incubation with the proteins (see Figure S7).

These results suggest that QD−dopamine conjugates can provide a means to probe dopaminergic neurotoxicity and neurodegeneration that are associated with oxidative metabolism of dopamine, depletion of biothiol molecules, and dysfunction of thiol proteins, such as parkin. The latter mediates the degradation of proteins toxic to dopaminergic neurons.[68−70]

Self-Assembly of Biotin-QDs with Streptavidin−Dye Conjugates. Our desire to apply biotin−streptavidin chemistry for bioconjugation is motivated by the ubiquitous use of such binding, due to its high-affinity interaction (dissociation constant $K_d^{-1} \sim 10^{-15}$ M) combined with its specificity and stability against pH changes and added salt.[10,71,72] This strategy is commonly applied via post-modification of the as-prepared nanoparticles with reactive biotin or streptavidin, followed by coupling to streptavidin- or biotin-labeled biomolecules.[19] Here, using a slightly different rationale, we introduced biotin groups in the ligand during synthesis starting with amine-biotin precursor. The activity of biotinylated QDs (prepared via photoligation with LA-PIMA-ZW/biotin) was tested by self-assembly with streptavidin prelabeled with *x*-rhodamine-isothiocyanate. This yields conjugates that can be tested via resonance energy transfer interactions.

Figure 5A shows the absorption spectra of QD-streptavidin-rhodamine at a dye-to-QD molar ratio from 0:1 to 12:1. There is a progressive increase in the absorption peak at ∼580 nm due to dye contribution. The corresponding composite emission spectra (using excitation at 400 nm) show a progressive loss in QD PL accompanied by a gradual increase in dye emission as the molar ratio increased (see Figure 5B). Since direct excitation of the dye is rather weak, we attribute the above changes to FRET quenching of the QD emission combined with sensitization of rhodamine. Values for the relative QD PL losses along with the FRET efficiencies, extracted from the deconvoluted spectra as a function of conjugate valence, are shown in Figure 5C. The trends for both experimental parameters agree with the predictions from the FRET interactions for a configuration of one central donor surrounded by n equally spaced acceptors. Using the expression of FRET efficiency for such conjugate configuration, $E = nR_0^6/(nR_0^6 + r^6)$, we extract an experimental estimate for $R_0 \cong 45.2$ Å and $r = 59.9$ Å; R_0 and r are the Förster radius and center-to-center separation distance, respectively. Additional details on conjugate formation and FRET analysis along with the corresponding parameters are provided in the Supporting Information (see Figure S8 and Table S1).

Click-Conjugation of Azido-QDs to DBCO-Transferrin and Intracellular Delivery. The alkyne−azide cycloaddition, referred to as "click" reaction, provides exquisite chemoselectivity and forms a stable triazole linker under mild reaction conditions.[53,73] This strategy has been used to functionalize various synthetic and biological molecules. In particular, the copper-free click reaction promotes effective conjugation of QDs to biomolecules without negative effects on the QD fluorescence.[40,74,75] Here, we demonstrate this approach by reacting azido-QDs (prepared via photoligation with LA-PIMA-ZW/N_3) with strained cyclooctyne labeled transferrin, producing highly luminescent QD-transferrin (QD-Tf) conjugates capable of entering live cells via receptor-mediated endocytosis.

Figure 6A,B shows epifluorescence images collected from HeLa cells incubated with green emitting QD-Tf (λ_{em} = 537 nm) and red emitting QD-Tf (λ_{em} = 633 nm) conjugates for 1 h. Images in each row of panels show differential interference contrast (DIC), DAPI staining of the nuclei (blue), QD emission (green/red) and merged images. The fluorescence images clearly show that coupling of transferrin to the QDs promoted the cellular uptake of the conjugates. Moreover, the QD fluorescence was dispersed in the perinuclear region, but no clear nuclear staining. In comparison, no intracellular QD fluorescence was observed when cells were incubated with QDs alone (in the absence of transferrin, see Figure S9). We further identified the distribution of the QD signal by coincubating the cells with an endosomal marker, Texas Red-labeled transferrin. Figure 6C shows that the distribution of green QD signal fully overlapped with the Texas Red signal, indicating that the QD-Tf was colocalized with the distribution of endo/lysosomal compartments. These results together strongly prove that transferrin conjugated to QDs promoted the cellular uptake, and internalization of the conjugates was driven by receptor-mediated endocytosis.

The cytotoxicity of these LA-PIMA-ZW ligated QDs has been assessed by incubating HeLa cell cultures for 24 h followed by performing MTT assay. We found that the viability of cells incubated with LA-PIMA-ZW-coated QDs remained high at 90−100% throughout the range of concentrations tested (0−100 nM, data not shown). This indicates that overall QDs capped with these zwitterion polymers induce little to no toxicity to cell cultures.

Polyhistidine-Mediated Self-Assembly of QD−Protein Conjugates. When possible conjugation of QDs and Au nanoparticles to biomolecules promoted by polyimidazole-to-metal coordination is easy to implement, and exploits the ubiquitous protocols of His-tagged protein expression in bacteria, or chemical synthesis of His-appended peptides.[28,76−79] This self-assembly route also allows control over the biomolecule orientation and the QD−conjugate valence. Several studies have shown that the key requirement for implementing such conjugation is to use compact capping ligands so that the His-tag on the biomolecule is able to directly access the nanocrystal surface.[8,19,76,77] Here, we investigate the self-assembly of His_7-tagged maltose binding protein (MBP-His_7) on QDs ligated with LA-PIMA-ZW. The conjugation was visually examined using affinity chromatography, which relies on the immobilization of conjugates onto an amylose column, followed by competitive release with soluble maltose (the substrate for MBP). As a positive control, we self-assembled MBP-His_7 onto LA-ZW-QDs and His-PIMA-ZW-QDs already tested in our previous work.[34] The ultimate goal is to test the effects of the nature of the capping ligands on the conjugation efficiency.

Thiol vs Imidazole Coordination. We tested side-by-side the self-assembly of MBP-His_7 onto QDs ligated with LA-PIMA-ZW and His-PIMA-ZW. A dispersion of LA-PIMA-ZW-QDs was incubated with MBP-His_7 for 30 min then loaded onto the

DOI: 10.1021/acs.bioconjchem.6b00309
Bioconjugate Chem. 2016, 27, 2024−2036

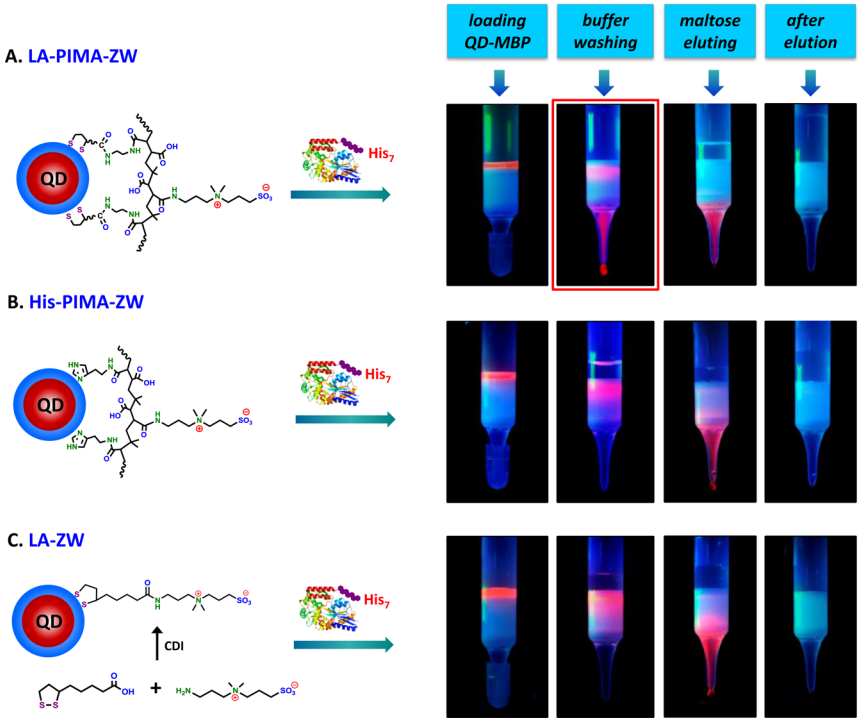

Figure 7. Amylose affinity chromatography assay testing the conjugation of MBP-His_7 to three sets of QDs ligated with LA-PIMA-ZW, His-PIMA-ZW, and LA-ZW, respectively. The His-PIMA-ZW ligand was described in our previous work;[34] the LA-ZW ligand was synthesized via CDI-coupling of lipoic acid with ZW-NH_2.

amylose column. This produced only a partial immobilization of the QD-conjugates as indicated by the red fluorescent band on top of the column observed under a hand-held UV lamp; most of the conjugates were eluted (see Figure 7A). Then, addition of 1 mL solution of 20 mM maltose readily eluted the fluorescent band. This result indicates that partial (incomplete) conjugation has taken place when QDs are coated with LA-PIMA-ZW. In comparison, when His-PIMA-ZW was used as capping ligands, incubation of the His-PIMA-ZW-QDs with MBP-His_7 produced a stable red fluorescent band on top of the column, which could not be eluted even after several washes with buffer. Addition of 1 mL of 20 mM D-maltose readily eluted the conjugates (see Figure 7B). This affinity chromatography assay, namely, binding to amylose and competitive release by soluble maltose, is consistent with the case of MBP-His_7 incubated with other size of QDs ligated with His-PIMA-ZW as reported in our previous work.[34] The difference in polyhistidine-driven conjugation of the MBP-His_7 onto these two sets of QDs can be attributed to a difference in the coordination of the anchoring groups (i.e., multi-imidazole vs multithiol) onto the QD surface. Coordination of imidazole on the QDs is weaker than that of thiol. Thus, the polyhistidine tag on the protein can compete for binding on the metal surface and induce rearrangement of the His-PIMA-ZW ligands, yielding stable QD-MBP conjugates. Conversely, though the zwitterion motif still allows the polyhistidine tag to reach to the QDs surface, it is not able to rearrange the LA-PIMA-ZW coating, which prevents stable conjugate formation.

Polymer versus Small Molecule Ligand. To investigate this effect, we tested the self-assembly of MBP-His_7 with QDs photoligated with LA-ZW (a molecular-scale ligand) and compared it to the case of LA-PIMA-ZW coating (above). This ligand was prepared by 1,1′-carbonyldiimidazole coupling of lipoic acid with ZW-NH_2, as detailed in the Supporting Information. The amylose column assay indicated that self-assembly of MBP-His_7 onto LA-ZW-QDs has taken place: conjugates tightly bound onto the amylose column, and were readily eluted with maltose (see Figure 7C). This result is attributed to the weaker coordinating affinity of bidentate ligand compared to the multithiol polymer, where ligand rearrangement allows the His-tagged protein to bind onto the QD surfaces.

Cumulatively, these results provide insight into the interplay between several parameters controlling the self-assembly. They indicate that the formation of QD-bioconjugates mediated by metal−polyhistidine coordination is not only determined by the compactness of the capping ligands, but is also greatly influenced by the strength of coordination onto the metal surface. These findings are greatly informative. They open additional possibilities for the future ligand design that can expand the application of this effective conjugation strategy to QDs and other metal-rich nanoparticles.

CONCLUSION

We expanded our earlier work, exploiting the effectiveness of the nucleophilic addition reaction to maleic anhydride, and synthesized a set of multilipoic acid coordinating polymers and applied them for the surface functionalization of luminescent QDs. Cap exchange with these polymers using a photoligation strategy has yielded hydrophilic QDs that exhibit excellent colloidal stability over a broad range of conditions, and which prevent nonspecific protein absorption. The flexibility of introducing various reactive groups into the ligands (carboxylic acid, amine, azide, and biotin) has facilitated the assembly of QD-bioconjugates using bio-orthogonal coupling strategies, including amine−isothiocyanate chemistry, biotin−streptavidin linkage, and copper-free click reaction. The produced QD-bioconjugates have been tested in a few representative

DOI: 10.1021/acs.bioconjchem.6b00309
Bioconjugate Chem. 2016, 27, 2024−2036

demonstrations highly relevant in biology, including sensing based on energy and charge transfer interactions and cellular imaging. Additionally, we used these ligands to investigate polyhistidine-mediated metal-affinity conjugation of protein onto QDs coated with three types of zwitterionic ligands. We showed that conjugation is equally influenced by the ligand size and strength of the metal-coordination onto the QD surfaces.

We should emphasize that the present chemical design can be easily applied to prepare ligands that are optimally adapted to coat a variety of metal and metal oxide nanomaterials, such as those made of gold, silver, and magnetic cores. Our design is also amenable to introducing biomolecules, such as peptides or proteins, directly into the ligand structures in situ, as these molecules naturally present amine functionalities.

Bioconjugates prepared with LA-PIMA-ZW-coated QDs and other nanoparticles provide versatile scaffolds with potential applications in an array of biological problems. These range from the imaging of blood vasculature and tracking of protein migration in live cells to in vitro and in vivo sensor design based on energy and/or charge transfer interactions.

EXPERIMENTAL SECTION

Synthesis of LA-PIMA-ZW (50% LA and 50% ZW). In a 50 mL three-neck round-bottom flask, 0.385 g of PIMA (MW ~6000 g/mol, 2.5 mmol of monomer units) was dissolved in 5 mL of DMSO. The solution was purged with nitrogen and heated to 50 °C. LA-NH_2 (0.31 g, 1.25 mmol) dissolved in 1 mL of DMSO was added to the PIMA solution via a syringe, followed by the addition of 1 mL of DMSO solution containing ZW-NH_2 (0.280 g, 1.25 mmol). The reaction mixture was left stirring at 50 °C overnight. The solution was concentrated to ~1 mL under vacuum, and 30 mL of acetone was added to precipitate the compound. After centrifugation of the mixture for 5 min at 3700 rpm, the solvent was decanted and the solid pellet was washed twice with chloroform, then dried under vacuum. This provided the final product as yellow solid; the final yield was ~87%.

Synthesis of LA-PIMA-ZW/R (R = 10% Azide, 10% Amine, or 10% Biotin). Synthesis of the reactive polymer ligands were carried out following the steps described above, except that 10% of the precursor ZW-NH_2 was substituted with R-NH_2 (where R = PEG-azide, PEG-amine, or biotin). Here, we detail the synthesis of azide-functionalized polymer ligand. The protocols for the synthesis of amine- and biotin-functionalized compounds are provided in Supporting Information. PIMA (0.385 g, 2.5 mmol of monomers) was dissolved in 5 mL of DMSO using a 50 mL round-bottom flask. The solution was purged with nitrogen and heated to 50 °C, and then 1 mL of DMSO containing LA-NH_2 (0.31 g, 1.25 mmol) was added using a syringe, followed by addition of 1 mL of DMSO containing H_2N-PEG-N_3 (0.156 g, 0.25 mmol) and ZW-NH_2 (0.224 g, 1 mmol). The mixture was left stirring overnight at 50 °C. The solvent was removed under vacuum and the compound was precipitated by adding 30 mL of acetone. After centrifugation, the solid pellet was washed with chloroform and dried under vacuum, yielding the final compound as yellow solid; the final yield was ~79%.

Photoligation of QDs. The ZnS-overcoated CdSe QDs used in this study were prepared following the protocols reported in the literature.[1,5,54] The syntheses of QDs was detailed in our previous work.[34] We focus on ligand exchange of hydrophobic QDs with LA-PIMA-ZW ligands. The same protocol can be applied to ligation of the QDs with LA-PIMA-ZW/N_3, LA-PIMA-ZW/NH_2, or LA-PIMA-ZW/biotin. The QD phase transfer to water was carried out in two steps: (1) coating with an intermediate ligand made of H_2N-PEG-OMe, followed by (2) photoligation with LA-PIMA-ZW.

Ligation with H_2N-PEG-OMe. A solution of hydrophobic TOP/TOPO-QDs (~26.7 μM, 150 μL) was precipitated with 3 mL of ethanol and redispersed in 150 μL of chloroform. Separately, 60 mg of H_2N-PEG-OMe was dissolved in 250 μL of chloroform. The ligand solution was then mixed with the QD dispersion in a scintillation vial. The vial was sealed with a rubber septum and the atmosphere was switched to nitrogen by applying 2 to 3 rounds of mild vacuum followed by purging with nitrogen. The mixture was then left stirring at room temperature for 3 h; alternatively one can apply overnight stirring at 4 °C. The QDs were precipitated by adding 5 mL of hexane. Following sonication for ~1 min, the solution was centrifuged at 3700 rpm for ~5 min, yielding a gel-like pellet. The pellet was dried under vacuum for ~10 min and redispersed in 200 μL of methanol.

Photoligation with LA-PIMA-ZW. In a separate vial, 15 mg of LA-PIMA-ZW was dissolved in 300 μL methanol, followed by the addition of 20 μL of fresh KOH aqueous solution (0.1 g/mL); a slight sonication (1−2 min) can accelerate ligand dissolution. This solution was mixed with the QD dispersion prepared in step one above, then 30 μL of tetramethylammonium hydroxide (~5 mM) predissolved in methanol was added. The vial was sealed with a rubber septum and the atmosphere was switched to nitrogen by applying 2 to 3 rounds of mild vacuum followed by flushing with nitrogen. The vial was then placed inside the UV photoreactor (peak at 350 nm, 4.5 mW/cm^2, Model LZC-4 V, Luzchem Research, Ottawa, Canada) and irradiated for 35 min while stirring.[64] The sample was retrieved and excess tetrahydrofuran was added to precipitate out the QDs, followed by sonication and centrifugation; the steps were repeated one more time. The resulting QD pallet was dried under vacuum and then dispersed in buffer (pH 12, 50 mM), yielding a clear aqueous dispersion; sonication for ~5 min can be applied to speed up the homogenization. The dispersion was filtered through a 0.45 μM syringe filter, and excess free ligands were removed by applying 3−4 rounds of concentration/dilution with DI water using a centrifugal filtration device (Millipore, MW cutoff = 50 kDa).

Conjugation of QDs to Dopamine. The QD−dopamine conjugates were prepared by reacting LA-PIMA-ZW/NH_2-QDs (10% amine) with dopamine-isothiocyanate (dopamine-ITC).[64] Briefly, 50 μL of dopamine-ITC predissolved in DMSO (0.5 mg/mL) was added to a scintillation vial containing 126 μL of QD dispersion (~6.35 μM) and 20 μL NaCl solution (1 M); DI water was added to bring the total volume to ~1 mL. The mixtures were stirred in the dark for ~3 h, and then one round of concentration/dilution was applied to remove the excess free/unreacted dopamine through a membrane filtration device (MW cutoff: 50 kDa, Millipore), providing 1 mL of the final conjugate dispersions (~0.8 μM).

pH-Dependent Quenching of the QD Fluorescence. The pH-dependent PL quenching data were collected from dilute dispersions, prepared by mixing 30 μL of the QD−dopamine conjugates with 470 μL of phosphate buffer (10 mM) at the desired pH. The integrated PL signal measured at each pH was reported relative to the value at pH 4.

QD PL Recovery Promoted by Cysteine Addition. Briefly, 30 μL of the QD−dopamine conjugates was mixed with 450 μL of phosphate buffer (10 mM, pH 10). Then 20 μL aliquots of

DOI: 10.1021/acs.bioconjchem.6b00309
Bioconjugate Chem. 2016, 27, 2024−2036

cysteine stock solution (0.2 mM) were added. The above dispersions were incubated for different time periods and the PL spectra were recorded.

Interaction of QD–Dopamine with BSA. 30 μL aliquots of QD–dopamine conjugates were dispersed in phosphate buffer (pH 10, 10 mM). Then, the desired volumes of BSA stock solution (0.1 mM) were added, and the final volume of the dispersions was adjusted to 500 μL by adding phosphate buffer. The BSA concentrations used in these measurements were 1, 2, and 3 μM. The PL spectra were recorded for each BSA concentration following different incubation time periods.

Self-Assembly of QD–Biotin with Streptavidin-Dye. Green-emitting QDs capped with LA-PIMA-ZW/biotin were used for self-assembly with streptavidin labeled with *x*-rhodamine-5-(and-6)-isothiocyanate (details about streptavidin labeling are provided in Supporting Information). The conjugates were prepared by incubating increasing molar ratios of the streptavidin-dye with the same concentration of the QDs. Briefly, 9 μL aliquots of a stock QD dispersion (8.57 μM) were loaded into Eppendorf tubes. The desired amount of a stock streptavidin-dye solution (7.1 μM) was mixed with QD dispersions; phosphate buffer (pH 7.5, 50 mM) was then added to bring the total volume to 400 μL. The ratio of streptavidin-dye-to-QD (i.e., valence) explored in this study was varied from 0:1 to 12:1. The mixtures were incubated at 4 °C for 1 h to allow for self-assembly, followed by collecting the absorption and emission spectra.

Click Conjugation of QD-Azide with DBCO-Transferrin. The QD–transferrin conjugates were prepared by reacting QD-LA-PIMA-ZW/N_3 with DBCO-transferrin. Two sets of QDs emitting at 537 and 633 nm were used. To prepare the green-emitting conjugates, 100 μL of LA-PIMA-ZW/N_3-capped QDs (6.28 μM) was first dispersed in 400 μL of DI water, then 50-fold excess of DBCO-transferrin solution (125 μL, 0.25 mM) was added while stirring. The mixture was left stirring at room temperature overnight. The QD–transferrin conjugates were purified from unreacted DBCO-transferrin using a PD-10 column. The same protocol was applied to prepare the red-emitting QD-conjugates, except that 100-fold excess of DBCO-transferrin with respect to QDs was used. The purified QD–transferrin conjugates were characterized using UV–vis spectroscopy and gel electrophoresis. The presence of transferrin was reflected in the contributions to the composite absorption spectra at ∼280 nm, while the gel images showed that after conjugation there was a reduction in mobility shifts in both green- and red-emitting QD–transferrin conjugates compared with those of QD-N_3 (control, see Figure S10).

Polyhistidine-Promoted QD-Protein Self-Assembly. Three sets of ligand-capped QDs (emitting at 633 nm) were used for conjugation: His-PIMA-ZW-QDs, LA-PIMA-ZW-QDs, and LA-ZW-QDs. The conjugation to maltose binding protein appended with a 7-histidine sequence (MBP-His_7) was carried out using the same protocol for all samples. Here we detail the assembly of LA-PIMA-ZW-QDs with MBP-His_7 at a molar ratio of 1:50. To an Eppendorf tube, ∼7.35 μL of QD dispersion (5.1 μM) was mixed with 37.5 μL of MBP-His_7 (50 μM), followed by addition of phosphate buffer (pH 8.0, 40 mM) to bring the total volume to 300 μL. The mixture was gently mixed then incubated at 4 °C for 30 min to allow for self-assembly. The integrity of the QD–protein conjugates was tested using affinity chromatography: binding to an amylose column followed by competitive release by amylose.

■ ASSOCIATED CONTENT

Supporting Information

The Supporting Information is available free of charge on the ACS Publications website at DOI: 10.1021/acs.bioconjchem.6b00309.

Materials, instrumentations, syntheses of ZW-NH_2, LA-NH_2, R-PEG-NH_2, biotin-NH_2, and LA-ZW, ^{1}H NMR characterization of ZW-NH_2, LA-NH_2, and biotin-NH_2, ^{1}H NMR spectrum of LA-PIMA-ZW-QDs, FT-IR spectrum of LA-PIMA-ZW/biotin-QDs, FRET analysis, labeling streptavidin with x-rhodamine-5-(and-6)-isothiocyanate, labeling transferrin with DBCO, absorption spectra of QD-transferrin conjugates, control experiment of cellular uptake of QDs alone (PDF)

■ AUTHOR INFORMATION

Corresponding Author

*E-mail: mattoussi@chem.fsu.edu.

Present Address

#Ocean Nanotech, LLC, 7964 Arjons Drive, San Diego, CA 92126

Notes

The authors declare no competing financial interest.

■ ACKNOWLEDGMENTS

The authors acknowledge FSU and the National Science Foundation for financial support (NSF-CHE #1508501 and #1058957). B.Z. acknowledges the Scientific and Technological Innovation Platform of Fujian Province (2014H2006) for financial support.

■ REFERENCES

(1) Murray, C. B., Norris, D. J., and Bawendi, M. G. (1993) Synthesis and Characterization of Nearly Monodisperse CdE (E = S, Se, Te) Semiconductor Nanocrystallites. *J. Am. Chem. Soc. 115*, 8706–8715.

(2) Hines, M. A., and Guyot-Sionnest, P. (1996) Synthesis and characterization of strongly luminescing ZnS-Capped CdSe nanocrystals. *J. Phys. Chem. 100*, 468–471.

(3) Alivisatos, A. P. (1996) Perspectives on the physical chemistry of semiconductor nanocrystals. *J. Phys. Chem. 100*, 13226–13239.

(4) Murray, C. B., Kagan, C. R., and Bawendi, M. G. (2000) Synthesis and characterization of monodisperse nanocrystals and close-packed nanocrystal assemblies. *Annu. Rev. Mater. Sci. 30*, 545–610.

(5) Peng, Z. A., and Peng, X. G. (2001) Formation of high-quality CdTe, CdSe, and CdS nanocrystals using CdO as precursor. *J. Am. Chem. Soc. 123*, 183–184.

(6) Talapin, D. V., Rogach, A. L., Kornowski, A., Haase, M., and Weller, H. (2001) Highly luminescent monodisperse CdSe and CdSe/ZnS nanocrystals synthesized in a hexadecylamine-trioctylphosphine oxide-trioctylphospine mixture. *Nano Lett. 1*, 207–211.

(7) Medintz, I. L., Uyeda, H. T., Goldman, E. R., and Mattoussi, H. (2005) Quantum dot bioconjugates for imaging, labelling and sensing. *Nat. Mater. 4*, 435–446.

(8) Mattoussi, H., Palui, G., and Na, H. B. (2012) Luminescent quantum dots as platforms for probing in vitro and in vivo biological processes. *Adv. Drug Delivery Rev. 64*, 138–166.

(9) Kim, C. S., Tonga, G. Y., Solfiell, D., and Rotello, V. M. (2013) Inorganic nanosystems for therapeutic delivery: status and prospects. *Adv. Drug Delivery Rev. 65*, 93–99.

(10) Sapsford, K. E., Algar, W. R., Berti, L., Gemmill, K. B., Casey, B. J., Oh, E., Stewart, M. H., and Medintz, I. L. (2013) Functionalizing Nanoparticles with Biological Molecules: Developing Chemistries that Facilitate Nanotechnology. *Chem. Rev. 113*, 1904–2074.

DOI: 10.1021/acs.bioconjchem.6b00309
Bioconjugate Chem. 2016, 27, 2024–2036

(11) Kairdolf, B. A., Smith, A. M., Stokes, T. H., Wang, M. D., Young, A. N., and Nie, S. M. (2013) Semiconductor Quantum Dots for Bioimaging and Biodiagnostic Applications. *Annu. Rev. Anal. Chem. 6*, 143−162.
(12) Howes, P. D., Chandrawati, R., and Stevens, M. M. (2014) Colloidal nanoparticles as advanced biological sensors. *Science 346*, 1247390.
(13) Lemon, C. M., Curtin, P. N., Somers, R. C., Greytak, A. B., Lanning, R. M., Jain, R. K., Bawendi, M. G., and Nocera, D. G. (2014) Metabolic Tumor Profiling with pH, Oxygen, and Glucose Chemosensors on a Quantum Dot Scaffold. *Inorg. Chem. 53*, 1900−1915.
(14) Silvi, S., and Credi, A. (2015) Luminescent sensors based on quantum dot-molecule conjugates. *Chem. Soc. Rev. 44*, 4275−4289.
(15) Zhou, J., Yang, Y., and Zhang, C. Y. (2015) Toward Biocompatible Semiconductor Quantum Dots: From Biosynthesis and Bioconjugation to Biomedical Application. *Chem. Rev. 115*, 11669−11717.
(16) Chinen, A. B., Guan, C. M., Ferrer, J. R., Barnaby, S. N., Merkel, T. J., and Mirkin, C. A. (2015) Nanoparticle Probes for the Detection of Cancer Biomarkers, Cells, and Tissues by Fluorescence. *Chem. Rev. 115*, 10530−10574.
(17) Ji, X., Wang, W. T., and Mattoussi, H. (2016) Controlling the spectroscopic properties of quantum dots via energy transfer and charge transfer interactions: Concepts and applications. *Nano Today 11*, 98−121.
(18) Mout, R., Moyano, D. F., Rana, S., and Rotello, V. M. (2012) Surface functionalization of nanoparticles for nanomedicine. *Chem. Soc. Rev. 41*, 2539−2544.
(19) Blanco-Canosa, J. B., Wu, M., Susumu, K., Petryayeva, E., Jennings, T. L., Dawson, P. E., Algar, W. R., and Medintz, I. L. (2014) Recent progress in the bioconjugation of quantum dots. *Coord. Chem. Rev. 263−264*, 101−137.
(20) Saha, K., Bajaj, A., Duncan, B., and Rotello, V. M. (2011) Beauty is skin deep: a surface monolayer perspective on nanoparticle interactions with cells and bio-macromolecules. *Small 7*, 1903−1918.
(21) Soenen, S. J., Parak, W. J., Rejman, J., and Manshian, B. (2015) Intra)cellular stability of inorganic nanoparticles: effects on cytotoxicity, particle functionality, and biomedical applications. *Chem. Rev. 115*, 2109−2135.
(22) Choi, H. S., Liu, W., Misra, P., Tanaka, E., Zimmer, J. P., Ipe, B. I., Bawendi, M. G., and Frangioni, J. V. (2007) Renal clearance of quantum dots. *Nat. Biotechnol. 25*, 1165−1170.
(23) Baker, M. (2010) Nanotechnology imaging probes: smaller and more stable. *Nat. Methods 7*, 957−962.
(24) Cai, E., Ge, P. H., Lee, S. H., Jeyifous, O., Wang, Y., Liu, Y. X., Wilson, K. M., Lim, S. J., Baird, M. A., Stone, J. E., et al. (2014) Stable Small Quantum Dots for Synaptic Receptor Tracking on Live Neurons. *Angew. Chem., Int. Ed. 53*, 12484−12488.
(25) Han, H. S., Martin, J. D., Lee, J., Harris, D. K., Fukumura, D., Jain, R. K., and Bawendi, M. (2013) Spatial charge configuration regulates nanoparticle transport and binding behavior in vivo. *Angew. Chem., Int. Ed. 52*, 1414−1419.
(26) Muro, E., Pons, T., Lequeux, N., Fragola, A., Sanson, N., Lenkei, Z., and Dubertret, B. (2010) Small and Stable Sulfobetaine Zwitterionic Quantum Dots for Functional Live-Cell Imaging. *J. Am. Chem. Soc. 132*, 4556−4557.
(27) Park, J., Nam, J., Won, N., Jin, H., Jung, S., Jung, S., Cho, S. H., and Kim, S. (2011) Compact and Stable Quantum Dots with Positive, Negative, or Zwitterionic Surface: Specific Cell Interactions and Non-Specific Adsorptions by the Surface Charges. *Adv. Funct. Mater. 21*, 1558−1566.
(28) Zhan, N. Q., Palui, G., Safi, M., Ji, X., and Mattoussi, H. (2013) Multidentate Zwitterionic Ligands Provide Compact and Highly Biocompatible Quantum Dots. *J. Am. Chem. Soc. 135*, 13786−13795.
(29) Sun, M. H., Yang, L. K., Jose, P., Wang, L., and Zweit, J. (2013) Functionalization of quantum dots with multidentate zwitterionic ligands: impact on cellular interactions and cytotoxicity. *J. Mater. Chem. B 1*, 6137−6146.
(30) Pombo Garcia, K., Zarschler, K., Barbaro, L., Barreto, J. A., O'Malley, W., Spiccia, L., Stephan, H., and Graham, B. (2014) Zwitterionic-coated "stealth" nanoparticles for biomedical applications: recent advances in countering biomolecular corona formation and uptake by the mononuclear phagocyte system. *Small 10*, 2516−2529.
(31) Susumu, K., Oh, E., Delehanty, J. B., Blanco-Canosa, J. B., Johnson, B. J., Jain, V., Hervey, W. J., Algar, W. R., Boeneman, K., Dawson, P. E., et al. (2011) Multifunctional Compact Zwitterionic Ligands for Preparing Robust Biocompatible Semiconductor Quantum Dots and Gold Nanoparticles. *J. Am. Chem. Soc. 133*, 9480−9496.
(32) Giovanelli, E., Muro, E., Sitbon, G., Hanafi, M., Pons, T., Dubertret, B., and Lequeux, N. (2012) Highly Enhanced Affinity of Multidentate versus Bidentate Zwitterionic Ligands for Long-Term Quantum Dot Bioimaging. *Langmuir 28*, 15177−15184.
(33) Tasso, M., Giovanelli, E., Zala, D., Bouccara, S., Fragola, A., Hanafi, M., Lenkei, Z., Pons, T., and Lequeux, N. (2015) Sulfobetaine-Vinylimidazole Block Copolymers: A Robust Quantum Dot Surface Chemistry Expanding Bioimaging's Horizons. *ACS Nano 9*, 11479−11489.
(34) Wang, W., Ji, X., Kapur, A., Zhang, C., and Mattoussi, H. (2015) A Multifunctional Polymer Combining the Imidazole and Zwitterion Motifs as a Biocompatible Compact Coating for Quantum Dots. *J. Am. Chem. Soc. 137*, 14158−14172.
(35) Yildiz, I., McCaughan, B., Cruickshank, S. F., Callan, J. F., and Raymo, F. M. (2009) Biocompatible CdSe-ZnS Core-Shell Quantum Dots Coated with Hydrophilic Polythiols. *Langmuir 25*, 7090−7096.
(36) Liu, W. H., Greytak, A. B., Lee, J., Wong, C. R., Park, J., Marshall, L. F., Jiang, W., Curtin, P. N., Ting, A. Y., Nocera, D. G., et al. (2010) Compact Biocompatible Quantum Dots via RAFT-Mediated Synthesis of Imidazole-Based Random Copolymer Ligand. *J. Am. Chem. Soc. 132*, 472−483.
(37) Viswanath, A., Shen, Y., Green, A. N., Tan, R., Greytak, A. B., and Benicewicz, B. C. (2014) Copolymerization and Synthesis of Multiply Binding Histamine Ligands for the Robust Functionalization of Quantum Dots. *Macromolecules 47*, 8137−8144.
(38) Susumu, K., Oh, E., Delehanty, J. B., Pinaud, F., Gemmill, K. B., Walper, S., Breger, J., Schroeder, M. J., Stewart, M. H., Jain, V., et al. (2014) A New Family of Pyridine-Appended Multidentate Polymers As Hydrophilic Surface Ligands for Preparing Stable Biocompatible Quantum Dots. *Chem. Mater. 26*, 5327−5344.
(39) Wang, W., Kapur, A., Ji, X., Safi, M., Palui, G., Palomo, V., Dawson, P. E., and Mattoussi, H. (2015) Photoligation of an amphiphilic polymer with mixed coordination provides compact and reactive quantum dots. *J. Am. Chem. Soc. 137*, 5438−5451.
(40) Zhao, X., Shen, Y., Adogla, E. A., Viswanath, A., Tan, R., Benicewicz, B. C., Greytak, A. B., Lin, Y., and Wang, Q. (2016) Surface labeling of enveloped virus with polymeric imidazole ligand-capped quantum dots via the metabolic incorporation of phospholipids into host cells. *J. Mater. Chem. B 4*, 2421−2427.
(41) Ma, L., Tu, C., Le, P., Chitoor, S., Lim, S. J., Zahid, M. U., Teng, K. W., Ge, P., Selvin, P. R., and Smith, A. M. (2016) Multidentate Polymer Coatings for Compact and Homogeneous Quantum Dots with Efficient Bioconjugation. *J. Am. Chem. Soc. 138*, 3382−3394.
(42) Palui, G., Avellini, T., Zhan, N. Q., Pan, F., Gray, D., Alabugin, I., and Mattoussi, H. (2012) Photoinduced Phase Transfer of Luminescent Quantum Dots to Polar and Aqueous Media. *J. Am. Chem. Soc. 134*, 16370−16378.
(43) Palui, G., Aldeek, F., Wang, W. T., and Mattoussi, H. (2015) Strategies for interfacing inorganic nanocrystals with biological systems based on polymer-coating. *Chem. Soc. Rev. 44*, 193−227.
(44) Biju, V. (2014) Chemical modifications and bioconjugate reactions of nanomaterials for sensing, imaging, drug delivery and therapy. *Chem. Soc. Rev. 43*, 744−764.
(45) Mizuhara, T., Moyano, D. F., and Rotello, V. M. (2016) Using the power of organic synthesis for engineering the interactions of nanoparticles with biological systems. *Nano Today 11*, 31−40.
(46) Susumu, K., Uyeda, H. T., Medintz, I. L., Pons, T., Delehanty, J. B., and Mattoussi, H. (2007) Enhancing the stability and biological

DOI: 10.1021/acs.bioconjchem.6b00309
Bioconjugate Chem. 2016, 27, 2024−2036

functionalities of quantum dots via compact multifunctional ligands. *J. Am. Chem. Soc. 129*, 13987−13996.
(47) Wang, W., Aldeek, F., Ji, X., Zeng, B., and Mattoussi, H. (2014) A multifunctional amphiphilic polymer as a platform for surface-functionalizing metallic and other inorganic nanostructures. *Faraday Discuss. 175*, 137−151.
(48) Wang, W., Ji, X., Na, H. B., Safi, M., Smith, A., Palui, G., Perez, J. M., and Mattoussi, H. (2014) Design of a Multi-Dopamine-Modified Polymer Ligand Optimally Suited for Interfacing Magnetic Nanoparticles with Biological Systems. *Langmuir 30*, 6197−6208.
(49) Aldeek, F., Hawkins, D., Palomo, V., Safi, M., Palui, G., Dawson, P. E., Alabugin, I., and Mattoussi, H. (2015) UV and Sunlight Driven Photoligation of Quantum Dots: Understanding the Photochemical Transformation of the Ligands. *J. Am. Chem. Soc. 137*, 2704−2714.
(50) Dai, M. Q., and Yung, L. Y. L. (2013) Ethylenediamine-Assisted Ligand Exchange and Phase Transfer of Oleophilic Quantum Dots: Stripping of Original Ligands and Preservation of Photoluminescence. *Chem. Mater. 25*, 2193−2201.
(51) Zylstra, J., Amey, J., Miska, N. J., Pang, L., Hine, C. R., Langer, J., Doyle, R. P., and Maye, M. M. (2011) A modular phase transfer and ligand exchange protocol for quantum dots. *Langmuir 27*, 4371−4379.
(52) Bullen, C., and Mulvaney, P. (2006) The effects of chemisorption on the luminescence of CdSe quantum dots. *Langmuir 22*, 3007−3013.
(53) Sletten, E. M., and Bertozzi, C. R. (2009) Bioorthogonal Chemistry: Fishing for Selectivity in a Sea of Functionality. *Angew. Chem., Int. Ed. 48*, 6974−6998.
(54) Dabbousi, B. O., RodriguezViejo, J., Mikulec, F. V., Heine, J. R., Mattoussi, H., Ober, R., Jensen, K. F., and Bawendi, M. G. (1997) CdSe)ZnS core-shell quantum dots: Synthesis and characterization of a size series of highly luminescent nanocrystallites. *J. Phys. Chem. B 101*, 9463−9475.
(55) Mattoussi, H., Cumming, A. W., Murray, C. B., Bawendi, M. G., and Ober, R. (1998) Properties of CdSe nanocrystal dispersions in the dilute regime: Structure and interparticle interactions. *Phys. Rev. B: Condens. Matter Mater. Phys. 58*, 7850−7863.
(56) Hens, Z., and Martins, J. C. (2013) A Solution NMR Toolbox for Characterizing the Surface Chemistry of Colloidal Nanocrystals. *Chem. Mater. 25*, 1211−1221.
(57) Einstein, A. (1905) The motion of elements suspended in static liquids as claimed in the molecular kinetic theory of heat. *Ann. Phys. 322*, 549−560.
(58) Edward, J. T. (1970) Molecular Volumes and Stokes-Einstein Equation. *J. Chem. Educ. 47*, 261.
(59) Lynch, I., and Dawson, K. A. (2008) Protein-nanoparticle interactions. *Nano Today 3*, 40−47.
(60) Mahmoudi, M., Lynch, I., Ejtehadi, M. R., Monopoli, M. P., Bombelli, F. B., and Laurent, S. (2011) Protein-Nanoparticle Interactions: Opportunities and Challenges. *Chem. Rev. 111*, 5610−5637.
(61) Treuel, L., Brandholt, S., Maffre, P., Wiegele, S., Shang, L., and Nienhaus, G. U. (2014) Impact of Protein Modification on the Protein Corona on Nanoparticles and Nanoparticle−Cell Interactions. *ACS Nano 8*, 503−513.
(62) Pelaz, B., del Pino, P., Maffre, P., Hartmann, R., Gallego, M., Rivera-Fernández, S., de la Fuente, J. M., Nienhaus, G. U., and Parak, W. J. (2015) Surface Functionalization of Nanoparticles with Polyethylene Glycol: Effects on Protein Adsorption and Cellular Uptake. *ACS Nano 9*, 6996−7008.
(63) Welsher, K., McManus, S. A., Hsia, C.-H., Yin, S., and Yang, H. (2015) Discovery of Protein- and DNA-Imperceptible Nanoparticle Hard Coating Using Gel-Based Reaction Tuning. *J. Am. Chem. Soc. 137*, 580−583.
(64) Ji, X., Palui, G., Avellini, T., Na, H. B., Yi, C. Y., Knappenberger, K. L., and Mattoussi, H. (2012) On the pH-Dependent Quenching of Quantum Dot Photoluminescence by Redox Active Dopamine. *J. Am. Chem. Soc. 134*, 6006−6017.
(65) Ji, X., Makarov, N. S., Wang, W. T., Palui, G., Robel, I., and Mattoussi, H. (2015) Tuning the Redox Coupling between Quantum Dots and Dopamine in Hybrid Nanoscale Assemblies. *J. Phys. Chem. C 119*, 3388−3399.
(66) Ji, X., Wang, W., and Mattoussi, H. (2015) Effects of separation distance on the charge transfer interactions in quantum dot-dopamine assemblies. *Phys. Chem. Chem. Phys. 17*, 10108−10117.
(67) Kraghhansen, U. (1981) Molecular Aspects of Ligand-Binding to Serum-Albumin. *Pharmacol. Rev. 33*, 17−53.
(68) Olanow, C. W., and Tatton, W. G. (1999) Etiology and pathogenesis of Parkinson's disease. *Annu. Rev. Neurosci. 22*, 123−144.
(69) LaVoie, M. J., Ostaszewski, B. L., Weihofen, A., Schlossmacher, M. G., and Selkoe, D. J. (2005) Dopamine covalently modifies and functionally inactivates parkin. *Nat. Med. 11*, 1214−1221.
(70) Sulzer, D., and Zecca, L. (1999) Intraneuronal dopamine-quinone synthesis: a review. *Neurotoxic. Res. 1*, 181−195.
(71) Weber, P. C., Ohlendorf, D. H., Wendoloski, J. J., and Salemme, F. R. (1989) Structural origins of high-affinity biotin binding to streptavidin. *Science 243*, 85−88.
(72) DeChancie, J., and Houk, K. N. (2007) The origins of femtomolar protein-ligand binding: hydrogen-bond cooperativity and desolvation energetics in the biotin-(strept)avidin binding site. *J. Am. Chem. Soc. 129*, 5419−5429.
(73) Debets, M. F., Van Berkel, S. S., Dommerholt, J., Dirks, A. J., Rutjes, F. P. J. T., and Van Delft, F. L. (2011) Bioconjugation with Strained Alkenes and Alkynes. *Acc. Chem. Res. 44*, 805−815.
(74) Bernardin, A., Cazet, A., Guyon, L., Delannoy, P., Vinet, F., Bonnaffe, D., and Texier, I. (2010) Copper-Free Click Chemistry for Highly Luminescent Quantum Dot Conjugates: Application to in Vivo Metabolic Imaging. *Bioconjugate Chem. 21*, 583−588.
(75) Schieber, C., Bestetti, A., Lim, J. P., Ryan, A. D., Nguyen, T. L., Eldridge, R., White, A. R., Gleeson, P. A., Donnelly, P. S., Williams, S. J., et al. (2012) Conjugation of Transferrin to Azide-Modified CdSe/ZnS Core-Shell Quantum Dots using Cyclooctyne Click Chemistry. *Angew. Chem., Int. Ed. 51*, 10523−10527.
(76) Medintz, I. L., Clapp, A. R., Mattoussi, H., Goldman, E. R., Fisher, B., and Mauro, J. M. (2003) Self-assembled nanoscale biosensors based on quantum dot FRET donors. *Nat. Mater. 2*, 630−638.
(77) Clapp, A. R., Medintz, I. L., Mauro, J. M., Fisher, B. R., Bawendi, M. G., and Mattoussi, H. (2004) Fluorescence resonance energy transfer between quantum dot donors and dye-labeled protein acceptors. *J. Am. Chem. Soc. 126*, 301−310.
(78) Dennis, A. M., Sotto, D. C., Mei, B. C., Medintz, I. L., Mattoussi, H., and Bao, G. (2010) Surface ligand effects on metal-affinity coordination to quantum dots: implications for nanoprobe self-assembly. *Bioconjugate Chem. 21*, 1160−1170.
(79) Lowe, S. B., Dick, J. A. G., Cohen, B. E., and Stevens, M. M. (2012) Multiplex Sensing of Protease and Kinase Enzyme Activity via Orthogonal Coupling of Quantum Dot Peptide Conjugates. *ACS Nano 6*, 851−857.

DOI: 10.1021/acs.bioconjchem.6b00309
Bioconjugate Chem. 2016, 27, 2024−2036